Geophysical Journal International

Geophys. J. Int. (2018) **214,** 148–163
Advance Access publication 2018 March 22
GJI Seismology

doi: 10.1093/gji/ggy107

High-frequency ground-motion parameters from weak-motion data in the Sicily Channel and surrounding regions

Sebastiano D'Amico,[1] Aybige Akinci[2] and Marta Pischiutta[2]

[1] *University of Malta, Msida MSD* 2080, *Malta*
[2] *Istituto Nazionale di Geofisica e Vulcanologia, Via di Vigna Murata 605, 00143, Rome, Italy. E-mail: marta.pischiutta@ingv.it*

Received 2018 January 15; in original form 2017 May 08

SUMMARY

In this paper we characterize the high-frequency (1.0–10 Hz) seismic wave crustal attenuation and the source excitation in the Sicily Channel and surrounding regions using background seismicity from weak-motion database. The data set includes 15 995 waveforms related to earthquakes having local magnitude ranging from 2.0 to 4.5 recorded between 2006 and 2012. The observed and predicted ground motions form the weak-motion data are evaluated in several narrow frequency bands from 0.25 to 20.0 Hz. The filtered observed peaks are regressed to specify a proper functional form for the regional attenuation, excitation and site specific term separately. The results are then used to calibrate effective theoretical attenuation and source excitation models using the random vibration theory. In the log–log domain, the regional seismic wave attenuation and the geometrical spreading coefficient are modelled together. The geometrical spreading coefficient, $g(r)$, modelled with a bilinear piecewise functional form and given as $g(r) \propto r^{-1.0}$ for the short distances ($r < 50$ km) and as $g(r) \propto r^{-0.8}$ for the larger distances ($r < 50$ km). A frequency-dependent quality factor, inverse of the seismic attenuation parameter, $Q(f) = 160f/f_{\mathrm{ref}}{}^{0.35}$ (where $f_{\mathrm{ref}} = 1.0$ Hz), is combined to the geometrical spreading. The source excitation terms are defined at a selected reference distance with a magnitude-independent roll-off spectral parameter, κ 0.04 s and with a Brune stress drop parameter increasing with moment magnitude, from $\Delta\sigma = 2$ MPa for $M_{\mathrm{w}} = 2.0$ to $\Delta\sigma = 13$ MPa for $M_{\mathrm{w}} = 4.5$. For events $M \leq 4.5$ (being $M_{\mathrm{wmax}} = 4.5$ available in the data set) the stress parameters are obtained by correlating the empirical/excitation source spectra with the Brune spectral model as function of magnitude. For the larger magnitudes (M_{w}>4.5) outside the range available in the calibration data set where we do not have recorded data, we extrapolate our results through the calibration of the stress parameters of the Brune source spectrum over the Bindi *et al.* ground-motion prediction equation selected as a reference model (hereafter also ITA10).

Finally, the weak-motion-based model parameters are used through a stochastic approach in order to predict a set of region specific spectral ground-motion parameters (peak ground acceleration, peak ground velocity, and 0.3 and 1.0 Hz spectral acceleration) relative to the generic rock site as a function of distance between 10 and 250 km and magnitude between *M* 2.0 and *M* 7.0.

Key words: Time Series Analysis; Earthquake Hazards; Earthquake Ground Motions; Seismic Attenuation; Wave Propagation..

INTRODUCTION

The study region of our interest accommodates the Sicily Channel as well as the Maltese Archipelago have experienced several large earthquakes with magnitudes up to 7.4, being epicentres mostly in Eastern Sicily and the Hellenic arc in the historical time. However, the rate of seismic activity in the region is relatively low, and there is almost no strong-motion recording especially for the Maltese Islands. Most of the hazard-related studies are limited to the Italian territory including only the Sicily Island as the southern-most area.

As it is well known, the detailed knowledge of regional attenuation versus distance relationship (indicating how the seismic propagation energy decreases with increasing distance) is essential for a complete improvement of the seismic hazard studies. In regions with

high seismicity, where strong ground motions are well recorded, the peak ground-motion displacement, velocity or acceleration decay curve with distance is empirically obtained from the recorded earthquakes (Douglas 2011).

Since such decay curves are empirically determined, they do not explicitly contain information about the attenuation manners of the seismic energy which, on the contrary, can be deduced by measurements based on a physical model of attenuation (Pisconti *et al.* 2015). These empirical equations called Ground Motion Predictive Equations (GMPE) allow estimating the seismic motion at a certain site by using simplified models in which the effect of seismic sources, propagation of seismic waves and site conditions are respectively represented by the magnitude, the distance from the source and geotechnical/geological site classification. Mostly these equations are derived by regressing strong-motion data, as the GMPEs developed in the framework of the NGA-West2 project (Abrahamson *et al.* 2014; Boore 2014; Bozorgnia *et al.* 2014; Campbell & Bozorgnia 2014; Chiou & Youngs 2014; Idriss 2014) and in the pan-European region by Akkar *et al.* (2014a, b), Bindi *et al.* (2014a, b) and Bora *et al.* (2015).

Unfortunately, a complete and sufficient set of strong-motion recordings that covers both the large magnitude and distance range is not always available in low-seismicity regions to properly constrain regression analyses. Usually, the simplest thing to do is choosing equations that have been derived from data acquired in areas with comparable geology, tectonics and seismicity since the regional variability of ground motion has been emphasized in several previous studies. For regions with the historical seismicity but insufficient recorded strong ground motions such as Central and Eastern North America, ground-motion predictions are generally theoretically or semi-empirically formulated (Pezeshk *et al.* 2011; NGA-East Project 2015). Moreover, numbers of paper have been published recently on determining some aspects of ground-motion scaling in several regions of the world by implementing large amounts of data using the background seismicity (e.g. Akinci *et al.* 2006; Atkinson & Boore 2006; Malagnini *et al.* 2007, 2012; Edwards *et al.* 2008; Rietbrock *et al.* 2013; Drout & Cotton 2010, 2015). Especially for low-seismicity regions, these studies have employed weak-motion recordings for deriving predictive relationships based on stochastic point- or finite-fault model. Such models are commonly used to simulate time histories and develop ground-motion equations (Atkinson & Boore 1995, 2006; Edwards & Fah 2013; NGA-East Project 2015).

For instance, in the Sicily Channel the largest local event (around 150 km to the Maltese Islands) recorded on fully digital instrumentation is M 5.0 with a hypocentral depth of 65 km. Because both the strong-motion data set and the seismicity are lacking in the region, we exploit a large number of weak-motion recordings from the background seismicity and calculate series of region-specific parameters to estimate earthquake-induced ground motions for future earthquakes in the Sicily Channel and the Maltese Islands. In fact, this work aims to address the use of the weak-motion data and properly predict future ground motions of high-magnitude earthquakes in the absence of the strong-motion recordings. In particular, we calculated following parameters: (i) anelastic regional attenuation function [Q factor as function of frequency and geometrical spreading coefficient, $g(r)$]; (ii) value of the average parameters that describes the attenuation of energy due to the most upper layers around the recording sites, $\kappa_;$ (iii) a functional form that characterizes the 'duration of shaking' as a function of distance and frequency; (iv) Brune stress drop parameter ($\Delta\sigma$) related to regional earthquakes and its variation with magnitude.

The ground-motion parameters in terms of peak ground acceleration (PGA), peak ground velocity (PGV) and spectral acceleration (SA) (0.3, and 1.0 Hz) are then computed through the random vibration theory (RVT) as a function of distance from the source between 10 and 250 km for a range of different moment magnitudes between M_w 2.0 and M_w 7.0 using a calibrated source model. RVT is the model and tool that requires signal duration and amplitude spectra at the recording site, and commonly used to predict the peak amplitudes of ground motion (Boore 1983). We combine the Brune spectral source model with our resulting regional attenuation model; duration of the ground motions coupled with site amplification factors proposed by Boore (2016) for the 'Generic-Rock Site' condition with the averaged velocity at 30 m depth, V_{s30}, is 760 m s^{-1} together with the decay slope of the source excitation at high frequencies (Anderson & Hough 1984). The moment magnitudes up to M 7.0 are much larger than the ones of the data set (M_{wmax}4.5) used to characterize source excitation and regional wave propagation. Extrapolations are retrieved over the calibration for the stress parameter of the Brune source spectrum, by comparing our weak-motion-based ground-motion estimations with a selected GMPE, derived by Bindi *et al.* (2011) as a reference model for magnitudes $M_w > 4.5$. We benefit the Italian Macroseismic Database to justify our ground-motion predictions for large earthquakes by using the relationship between the Mercalli–Cancani–Sieberg macroseismic intensity (IMCS) and PGA values proposed by Locati *et al.* (2016).

STRUCTURAL SETTING AND SEISMICITY OF THE SICILY CHANNEL

The Sicily Channel and eastern Sicily are among the most seismically active regions of the entire Mediterranean (D'Amico *et al.* 2013; Baccheschi & D'Amico 2014 and reference in therein). The complex tectonic framework is mainly controlled by the collision between the Eurasian and African plates (Finetti 1982; Cello *et al.* 1985; Reuther & Eisbacher 1985). In particular, the Strait of Sicily Rift is a fault-controlled and elongated trough in the foreland of the Sicilian Apennine-Maghrebian fold belt and thrust (Fig. 1). The largest faults that opened the Strait of Sicily Rift accommodate throws of >2 km and developed an exceptionally deep seafloor bathymetry, characterized by a stepped seafloor topography, that exceeds 1 km in depth. The maximum activity phase in the development of the Rift occurred during Plio-Quaternary times (Dart *et al.* 1993) and produced the trough as well as the uplift of the northern rift flank that produced the emergence of the Maltese Archipelago in early Messinian (Pedley 1987). Seismic reflection data have suggested syn-rift normal fault activity <5 Ma showing significant stratigraphic thickness changes fault-related (Dart *et al.* 1993). The most important active fault system appears to be the off-shore, striking ESE–WNW and paralleling the Strait of Sicily Rift. The on-shore northernmost extent of the Rift fault system, located on the SW coast of Malta, is supposed to be active during late Pleistocene-Holocene (Bonson *et al.* 2007). Differently, the majority of on-shore faults of the Maltese Archipelago strikes ENE–WSW and their neotectonic movements have not yet been neither reported nor deeply investigated.

In this region a high number of seismic events with magnitude higher than 7.0 is contained in historical Italian earthquake catalogues (CPT11, Rovida *et al.* 2011). Moreover, in this region took place the most devastating Italian tsunamis, as shown by tsunami catalogues (Tinti *et al.* 2004). Waves locally exceeding 10 m were produced in the tsunamis caused by the earthquakes of 1693 January

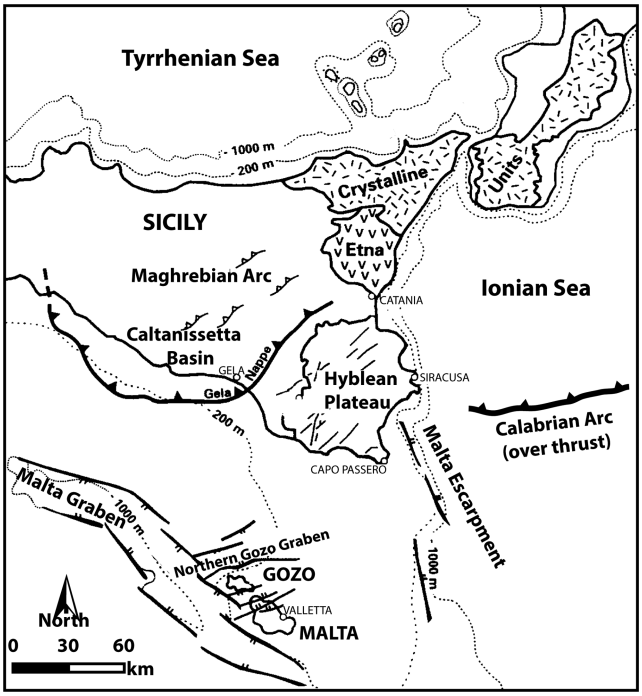

Figure 1. Tectonic map of the Sicily Channel and Central Mediterranean together with the main geological and physiographic features of Sicily Channel and Maltese Islands (modified after Gardiner *et al.* 1995).

11 and of 1908 December 28, hitting eastern Sicily and the Messina Straits, respectively. Based on morphotectonic arguments and off-shore seismic data analysis (Bianca *et al.* 1999; Argnani & Bonazzi 2005), as well as tsunami scenarios through the numerical simulations (Tinti *et al.* 2001; Tinti & Armigliato 2003), several authors have subsequently proposed that the causative faults are related to Malta escarpment in the off-shore of eastern Sicily, characterized by active extensional tectonics.

Moreover, there have been seven strong earthquakes reported in Malta, the last in 1923 which has caused some damage in the Maltese islands (Galea 2007). Finally, we stress that also Eastern Sicily, that is one of the most seismically active areas in the Sicily Channel, has been experienced by least five destructive earthquakes in the last 1000 years (1169, 1542, 1624, 1693, 1818) with magnitudes between 5.5 and 7.4 (Boschi *et al.* 1995).

DATA SET AND METHODOLOGY

We used background seismicity and earthquake data recorded at 48 broad-band seismic stations of the Italian Seismic Network (ISN) run by Istituto Nazionale di Geofisica and Vulcanologia (INGV) that recorded about 1968 earthquakes in the region from 2006 and 2012. In particular, we used 15 995 waveforms related to earthquakes having local magnitude ranging from 2.0 to 4.5, the bulk of data being concentrated between M 2.0 and M 2.5. The selected events were recorded at epicentral distances between 5 and 250 km. Figs 2 and 3(a) and (b) show the epicentral distribution and the characteristic of the used data set, respectively.

In this study we follow the methodology proposed by Raoof *et al.* (1999), Malagnini & Hermann (2000) and Malagnini *et al.* (2000), and refer the reader interested in details of the methodology to these papers. The approach has been successfully applied in several regions worldwide (Akinci *et al.* 2006, 2014; D'Amico

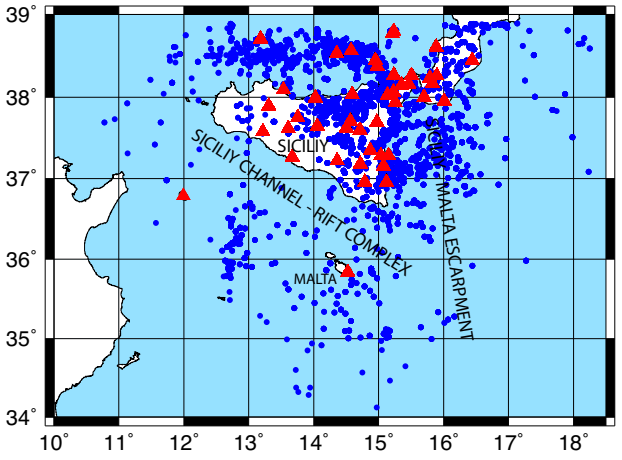

Figure 2. Regional map of the study area. The grey circles and triangles present the epicentral locations of the earthquakes and the locations of the Istituto Nazionale di Geofisica e Vulcanologia (INGV) seismic station that are used for the regression analysis, respectively.

et al. 2012, and references herein). These authors demonstrated how the large amount of regional and local seismic network data can be used for calibration of models for stochastic predictions of the ground motions in regions where the seismicity is moderate and where strong-motion records are rare. They pointed out the importance of uncertainties in the seismic wave propagation and their impact on the earthquake hazard analysis. This paper has been aimed in this respect towards developing new and reliable relations for studying region using the calibrated theoretical method of stochastic ω-square prediction. Random vibration model of earthquake ground motions uses Brune's spectra (Brune 1970, 1971), together with simple, but physically sound assumptions about geometrical spreading and anelastic attenuation to present the Fourier amplitude of ground motion due to shear waves. Using this spectrum and associated duration, one calculates the root mean square (rms) and peak amplitudes of ground response by assuming that the ground motion during the strong shaking portion of an earthquake is a finite-duration segment of a Gaussian random process.

For the purpose of this study an extensive database was used following the quality and reliability analysis and digital data processing. First of all, each waveform was visually investigated in order to avoid recordings with low signal-to-noise ratio. Signals were corrected for the instrument response and converted to ground velocity in meters per seconds. Then, the pickings of the P- and S-wave arrivals were analysed. Finally, corrected time-series were filtered around 14 central frequencies f_c (0.25, 0.40, 0.60, 0.85, 1.25, 1.75, 2.5, 3.5, 5.0, 7.0, 9.0, 12.5, 17.5, and 20.0 Hz). We have combined a low-pass and a high-pass filter with corner frequency at $\sqrt{2}\,f_c$, both 8-pole Butterworth

For each filtering frequency band and for each event, the peak amplitudes of the velocity time-series were evaluated in the time domain. All the velocity peak values $peak(a(f_c, r_{ij}))$, for each f_c at the jth site during the ith event, are gathered into a matrix using the following representation and be can be separated as the effect of source, site, and propagation path (e.g. Andrews 1986; Phillips & Aki 1986; Iwata & Irikura 1988; Castro *et al.* 1990; Boatwright *et al.* 1991; Hartzell 1992; Carver & Hartzell 1995; Raoof *et al.* 1999):

$$A_{ij}\left(f_c, r_{ij}\right) = \mathrm{EXC}_i\left(f_c, r_{\mathrm{ref}}\right) + \mathrm{SITE}_j\left(f_c\right) + D\left(r_{ij}, r_{\mathrm{ref}}, f_c\right) \qquad (1)$$

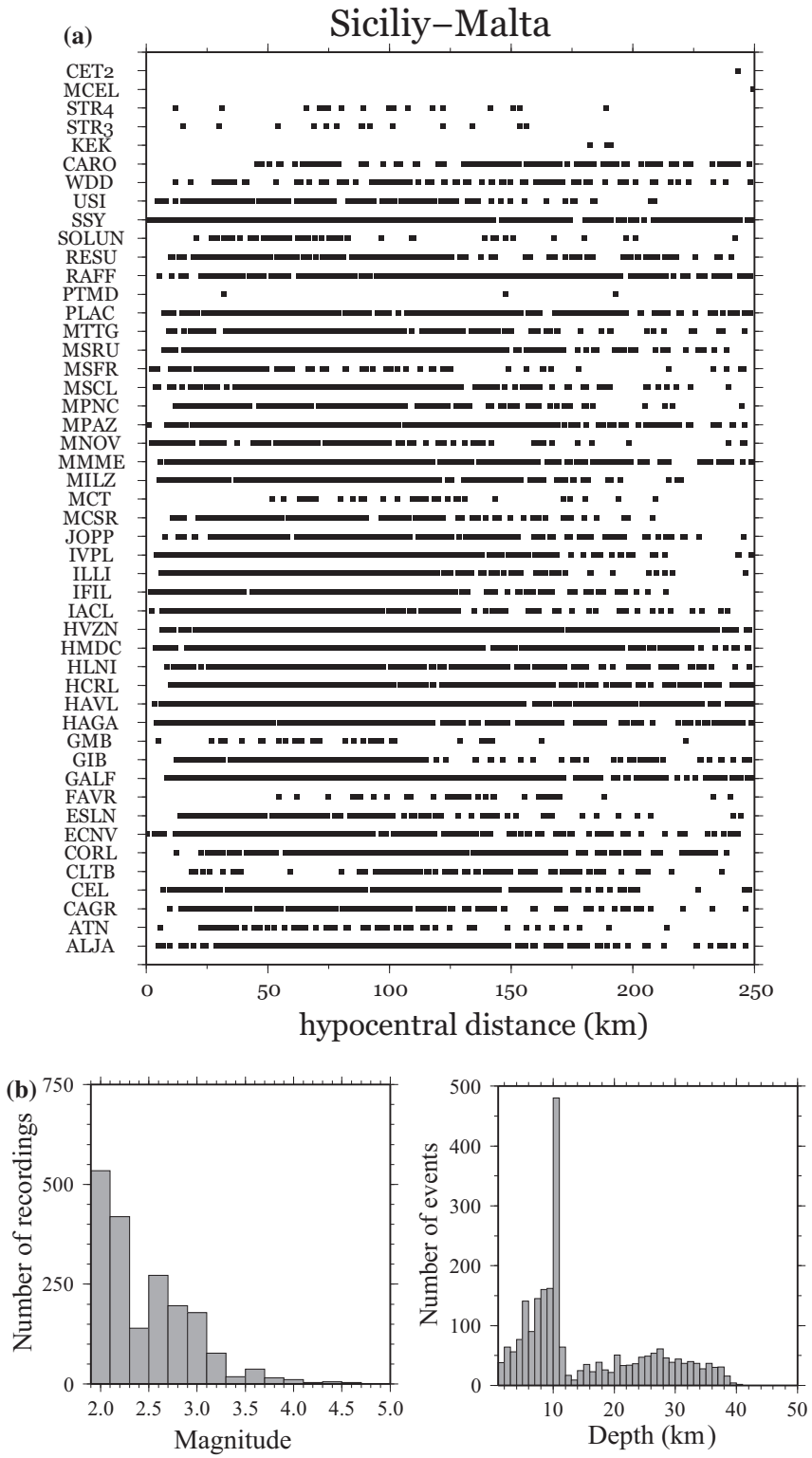

Figure 3. (a) Source–receiver distances distribution used for the regression analysis. (b) Number of earthquakes (used weak-motion data) as a function of magnitude and depth.

where r represents the hypocentral distance, A_{ij} $(f_c, r_{ij}) = \log_{10}(peak(a(f_c, r_{ij})))$ is the maximum peak (in velocity) of the recorded ground motion, SITE_j (f_c) and EXC_i (f_c, r_{ref}) represent the site term and the source term respectively. $D(r_{ij}, r_{ref}, f_c)$ is the regional seismic wave attenuation including the geometrical spreading coefficient and frequency dependent anelastic attenuation. L1-norm inversion method is used to solve eq. (1). In order to reduce the degrees of freedom some constraints are applied to stabilize the regressions.

In order to force the crustal attenuation term to be zero at an attributed distance, as well as the sum of the site effects at particular frequency and at an attributed distance, $r_{\rm ref} = 40$ km and defined as follows:

$$D(r = r_{\rm ref}, f_{\rm c}) = 0.0 \quad (2)$$

$$\sum \mathrm{SITE}_j\,(f_{\rm c}) = 0.0. \quad (3)$$

The reference distance r_{ref} is chosen to be greater than the hypocentral depth of the events used in the database. In this way the average absolute site effects (Malagnini *et al.* 2004) are accomplished and introduced to the source excitation spectra $\mathrm{EXC}_i(f_{\rm c}, r_{\rm ref})$. This is the reason we called this term as the "source excitation" rather than the "absolute source". Therefore, the $\mathrm{EXC}_i\ (f_{\rm c}, r_{\rm ref})$ represents the ground-motion level expected at this reference distance at the averaged network site effects. In this way the wave propagation term $D\ (r, f)$ is not disturbed by the presence of the regional amplifications. Additionally, the smoothing constraint was enforced to the crustal attenuation term $D(r_{ij}, r_{\rm ref}, f_c)$, imposing a constraint of minimum roughness with a null second derivative. It is outlined over the segmented distances:

$$D\,(r, r_{\rm ref}, f_{\rm c}) = \sum_{m=1}^{N\mathrm{nodes}} L_m(r) D_m \quad (4)$$

in which $L_m\ (r)$ is a linear interpolation function, m is the nodes for the distance segments and D_m is the chosen value for the attenuation function at the hypocentral distance. We constantly sampled the data set using a logarithm scale, selecting specific distances for each node.

In this study, model matrix (eq. 1) is constructed at around fourteen central frequencies as mentioned above. Regressions carried out all over the central frequencies represent the terms $\mathrm{EXC}_i\ (f_{\rm c}, r_{\rm ref}\ )$, $\mathrm{SITE}_j\ (f_{\rm c})$, $\mathrm{D}(r_{\rm ij}, r_{\rm ref}, f_{\rm c})$ using an L1-norm inversion scheme as described by Bartels & Conn (1980). Regression results are given for each term; path, source and site (eq. 1) separately in Figs 4, 5(a) and (b) and 6, respectively (empirical regression results are presented by black curves in each figure). We also calculated the effective time duration using time window containing the 5% and 75% of seismic energy following the *S*-wave arrival. These durations are presented in Fig. 7 as a function of distance at the six frequency bands. The signal duration is an important and a necessary parameter for the ground-motion prediction and can play an important role for earthquake damage potential and for engineering purposes especially in the assessment of liquefaction potential and the inelastic deformation and energy dissipation of the short-period structures (Bommer & Martinez-Pereira 1999; Mahin 1980). This parameter will be used later in our study to predict the peak values of the time series which is required by RVT application (see the following section).

HIGH-FREQUENCY GROUND-MOTION SCALING AND MODELLING

The most important parameters or assumption in the random vibration modelling are the stress drop $\Delta\sigma$ (and its dependence with magnitude), functional form of anelastic attenuation $1/Q(f)$ and geometrical spreading coefficient $g(r)$, near-site attenuation term κ and duration T. The modelling procedure can be performed again following the RVT and the stochastic simulations (Boore & Joyner 1984; Boore 1983, 2005) considering the spectral amplitude shape

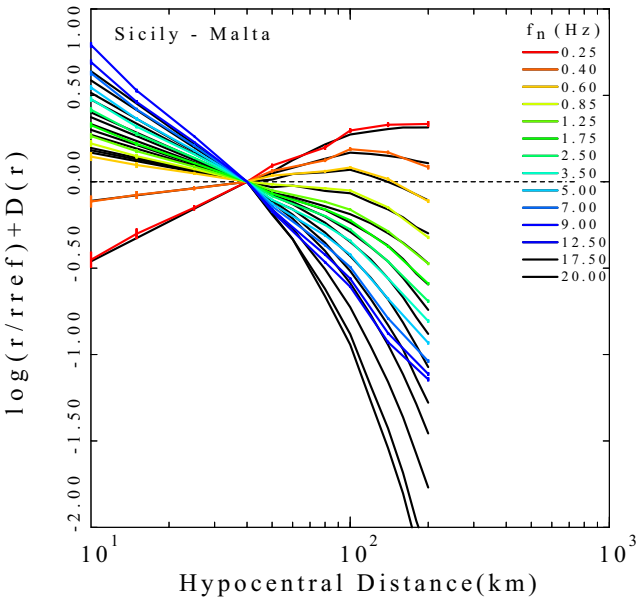

Figure 4. Empirical propagation terms at $f_{\rm c}$ (coloured curves) as a results of regression of velocity waveform peaks. The attenuation and site term were set to zero at the reference distance of 40 km. Our theoretical predictions (black lines) were obtained for each $f_{\rm c}$ using RVT. Finally, the horizontal dashed line indicates the frequency dependence of the filtered time domain $D(r)$ corrected for the geometrical spreading coefficient.

and the signal duration to predict PGA, PGV and response spectra. So that three main outcomes of the regression analysis (path, source and site related terms) are modelled by the proper functional forms.

The term $D(r_{ij}, r_{\rm ref}, f_{\rm c})$ is modelled by defining the anelastic attenuation parameters $Q(f) = Q_{\rm o}(f/f_{\rm ref})$ and geometrical spreading $g(r)$ (Aki 1980), together with the frequency and distance dependent duration (Fig.3). It is important to note that there is a trade-off between the anelastic attenuation and the geometrical spreading, and it is hard to be distinguished and exist several methods to aim to jointly solve both parameters (de Lorenzo *et al.* 2013). The $r_{\rm ref}$ is chosen such that misallocations in hypocentral depth would not significantly change the reference hypocentral distance. The seismic source excitation $\mathrm{EXC}_i\ (f_{\rm c}, r_{\rm ref}\ )$ in our data set is modelled using the Brune's source spectrum with a stress drop parameter $\Delta\sigma$ as a function of magnitude. For the near site attenuation κ an independent site term is attributed to each and every specific component of the ground motion, for all stations. Since we forced the sum of the site terms $\mathrm{SITE}_j\ (f_{\rm c})$ to a null value in the inversion matrix, our final site terms present the relative site effects to the network average and are automatically projected into the individual excitation terms in the source spectra.

Anelastic attenuation and geometrical spreading

Fig. 4 shows the results of the regression as attenuation term as a function of frequency and distance. Our empirical predictions for the crustal attenuation terms are given in Fig. 4 as a function of different central frequencies with coloured curves. These curves present the normalized attenuation functions as a deviation from a $1/r$ trend (horizontal lines in the figure represent a decay $1/r$). However, the theoretical predictions of the attenuation functions are presented by black lines obtained for each central frequency through RVT, considering a spectral model and calculated durations as a function frequency (see Fig. 7). The crustal wave propagation is described

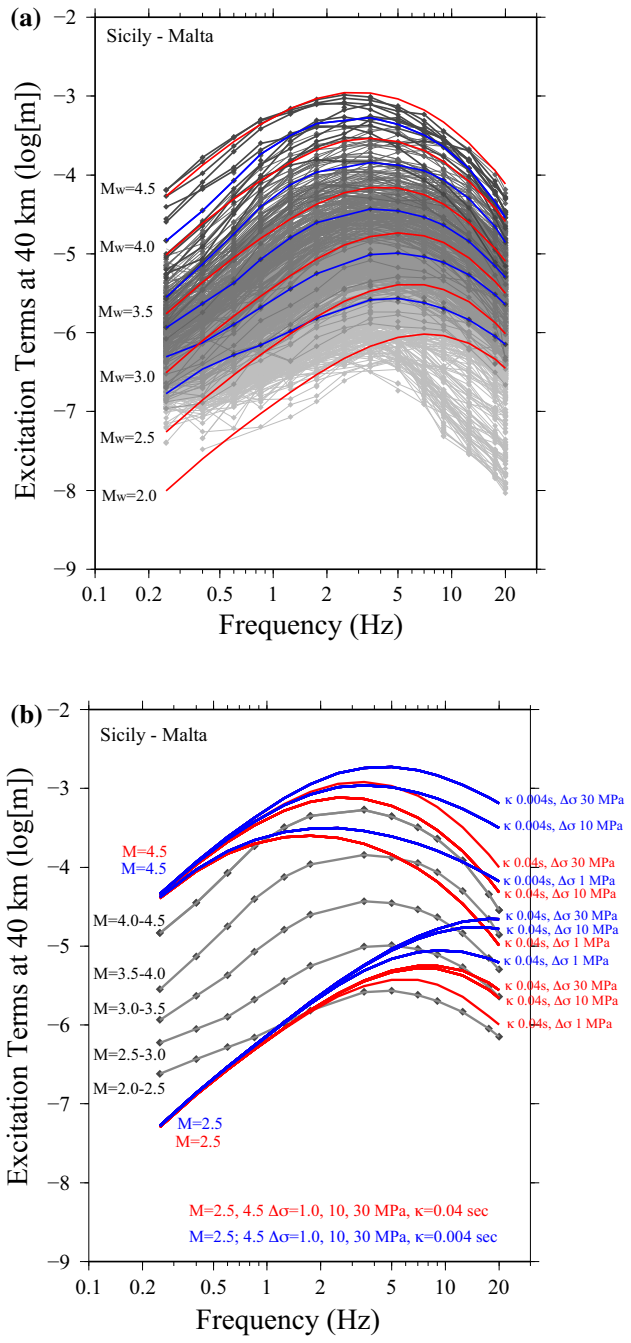

Figure 5. Excitation of the peak-filtered velocities at a reference distance $r_{ref} = 40$ km. (a) Comparison between the excitation terms of all earthquakes with magnitudes between 2.5 and 4.5 with predictions obtained through the RVT. The theoretical source terms computed for magnitudes of 2.5, 3.0, 3.5, 4.0 and 4.5 are indicated through red curves. The average excitation terms computed for magnitude ranges between 2.0 and 2.5, 2.5 and 3.0, 3.0 and 3.5, 3.5 and 4.0, and 4.0 and 4.5 are indicated through blue curves. (b) Trade-off existing between $\Delta\sigma$ and κ. Velocity spectra at two reference magnitudes ($M_{ww\ 1980)2.0}$ 2.0 and M_w 4.5) are shown. They were derived by the Brune spectral model applying three different values for the stress parameter $\Delta\sigma$, and two different values of the high-frequency attenuation parameter κ. Spectra propagation from the source to the reference distance (40 km) is performed considering the propagation characteristics of the region. The two values of κ generically refer to rock sites (0.004 s), and to moderately attenuating sites (0.04 s). Finally, the three values of stress parameter (1, 10 and 30 MPa) are within a normal range of variability.

following a functional form that combines the frequency-dependent attenuation and the geometrical spreading coefficient and given as (Boore 2003):

$$D(r, r_{ref}, f_c) = \log\{g(r)\} - \log\{g(r_{ref})\} - [\pi f_c(r - r_{ref})\log e/\beta Q_0(f/f_{ref})^{\eta}]. \quad (5)$$

We then find our preferred high-frequency ground-motion attenuation model using a trial-and-error procedure in fitting the observed decay curves it is neither possible nor necessary to fit each curve well. The best fit between the theoretical and the empirical curves is satisfied by using the following parameters and relations eqs (6) and (7) (Knopoff & Hudson 1967; Newman 1973; Aki 1981; Mitchell 1981):

$$Q(f) = 160(f/f_{ref})^{0.35}, \quad (6)$$

where $f_{ref} = 1.0$ Hz, with the bilinear relationships for the hinged-trilinear regional geometrical spreading parameter

$$g(r) = r^{-1.00} \quad r \le r_0 = 50\,\text{km}$$

$$g(r) = (1/r_o)(r_o/r)^{0.8} \quad r > r_o. \quad (7)$$

The crossover distance 50 km is related to the supercritical incidence of shear waves reflecting off the Moho and marks the transition between body- and surface-wave geometrical spreading. For distances shorter than the crossover, the regional geometrical spreading parameter is related to the body wave propagations and generally is accepted to be r^{-1}. For distances beyond 50 km, the latter parameter *g(r)* requires a smoother value $r^{-0.8}$ than the theoretical expected one ($r^{-0.5}$) for surface waves. However, it is obtained $r^{-1.0}$ for the shorter distance, which is similar to the expected value for the body-waves propagation in the crustal. We ascribe this smooth change (see change of rate of amplitude decay in the attenuation function in Fig. 4) in the exponent coefficient to several possible causes, as: (i) there is no clear transit between lower crust and Moho and the border between the fall-off of direct waves is not pronounced; (ii) the contribution of the SmS phases is weak; (iii) the emergence of lower crustal or Moho reflections is not significant (Aki & Richards 2002).

The excitation source term

The empirical excitation terms, EXC_i *(*f_c, r_{ref}) in eq. (1) are linked to the source spectrum and they represent the average expected level of ground motion at reference distance, r_{ref} for each earthquake. These terms can be modelled using the Brune (1970, 1971) spectrum and "propagating" the source at the hypocentral reference distance of 40 km:

$$s(f, M_w)(1/r_{ref})\exp(-\pi r_{ref}\beta) \times Q_o(f/f_{ref})^{\eta}\langle V(f)\exp(-\pi f\kappa_o)\rangle_{avg}, \quad (8)$$

where the term *V(f)* expresses the average amplification site at the bedrock (Atkinson & Silva 1997). κ_o describes the spectral decay at high frequency at the recording site (Anderson & Hough 1984). It may be also defined as the near-surface high-frequency attenuation parameter. Since the geologic site conditions as well as the velocity profile are not known for the recording stations in our study, the average modification of the signal due to the site are controlled by the term $\langle V(f)\exp(-\pi f\kappa_o)\rangle$. This latter may be written as κ_{eff} which represents the average distortion induced by the network

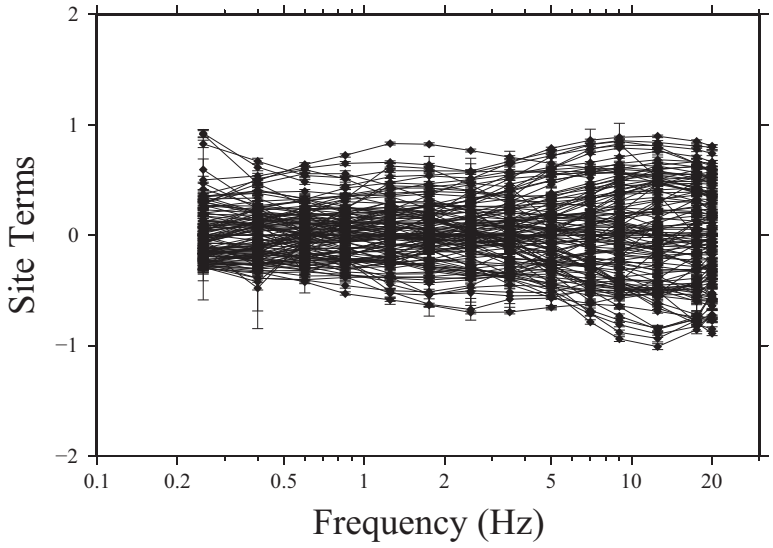

Figure 6. The site terms, derived from the regressions of horizontal peak-filtered velocities, are shown with black lines.

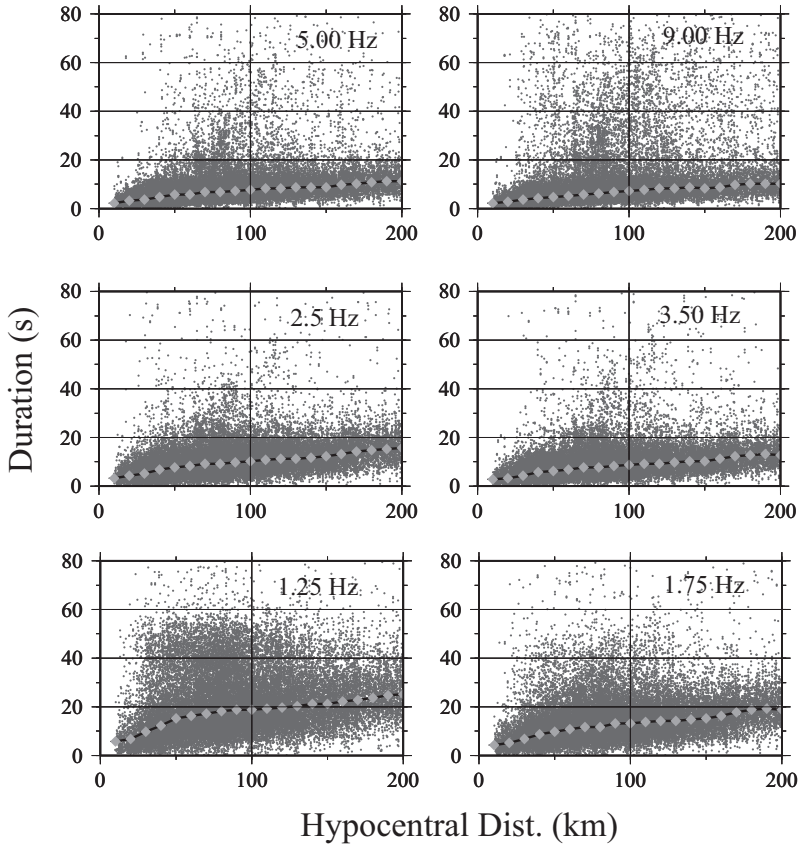

Figure 7. At selected frequencies we report durations of seismic signals together with their standard errors as a function of distance. For each seismogram the duration is calculated with time windows containing the 5%–75% of the integrated seismic energy that follows the onset of the *S*-wave. Black squares indicate the duration estimates computed for each recording, while grey diamonds indicate the L1-norm estimates of the duration function that were used in RVT analysis for the prediction of peak amplitudes. A piecewise linear curve (black) is used to link the grey diamonds.

sites:

$$\exp(-\pi f \kappa_{\text{eff}}) \sim \langle V(f) \exp(-\pi f \kappa_{\text{o}}) \rangle_{\text{avg}}. \quad (9)$$

The Fourier velocity spectra is represented by the following form of $s(f, M_{\text{w}})$:

where M_{o} is the seismic moment (in Nm, according to Hanks & Kanamori 1979), expressed by $\log M_{\text{o}} = 1.5(M_{\text{w}} + 6.03)$, ρ is the density at the source and β is the shear-wave velocity at the source. Moreover, $K = R_{\Theta\Phi} \times V \times F = 0.55 \times 0.707 \times 2.0$ is a coefficient composed of the effects of the radiation pattern ($R_{\Theta\Phi}$),

the free-surface effect for vertically incident *S* waves (*F*), and the energy partition of initial shear wave amplitude (*V*).

Thus, the one-corner source spectrum $S(f)$ is given bywhere $f_c = 0.49\beta(\Delta\sigma/M_o)^{1/3}$. Here the corner frequency *fc* is determined from the spectra. It is related to: the stress drop, $\Delta\sigma$ (MPa), seismic moment M_o (Nm) and the shear wave velocity β (ms^{-1}). The constant 0.49 depends on the type of model spectra and the geometry of the source.

The empirical excitation source spectra are given in Fig. 5(a) (black lines) together with the averaged source spectra (grey lines) for events with magnitudes range between *M* 2.0 and *M* 2.5, *M* 2.5 and *M* 3.0 up to the *M* 4.0 and *M* 4.5. Empirical source spectra are obtained over the regressions of the filtered peak amplitudes and the theoretical models (red lines), that are obtained using the equation described above. The theoretical curves were accessed by combining the source contribution (given by the Brune spectral model), the regional geometric/anelastic attenuation, and the adopted site amplification. This latter is given by the term V(*f*), and was arbitrarily chosen as a generic rock site (e.g. Boore 2016) which corresponds to $V_{s30} = 760$ m s^{-1}. The amplification factors used in our study were derived applying the quarter-wavelength approach (e.g. Boore & Joyner 1997). Finally, in order to reproduce the spectral decay at high frequencies due to scattering and attenuation at the site, we have also applied a high frequency filter defined through an attenuation term (κ parameter, chosen to be equal to 0.04 s). We also consider the estimated frequency-specific duration values (Fig. 7), at the 40 km reference distance for the RVT simulations of the filtered peak ground velocities.

There exists a trade-off between κ and $\Delta\sigma$ in defining the radiated energy at the source. In this study the site and the source terms present the averaged regional responses taking into account all the sampled azimuths and incidence angles from the surface to the bedrock depth, over all the sites as a result of the applied regression method. Therefore, in this study we defined a stress drop $\Delta\sigma = 2$ MPa for $M_w = 2.0$ events and $\kappa = 0.04$ s, the latter is not dependent of seismic moment, besides dependents only on the average attenuation properties at the recording sites. κ-values scatter as an effect of the subsurface geology, and seem to be smaller at rock sites than on soft sediments or on soft rocks. However, the absolute scaling at the source and the absolute site effects may be properly computed in a separate study (Malagnini *et al.* 2004; 2007; 2014a, b).

From Fig. 5(a) it is possible to notice that the fit for M_w greater than 4.0 events are very good at every frequency. Furthermore, we observed that the stress drop increases linearly with the magnitude from $\Delta\sigma = 2$ MPa for $M_w = 2.0$ to $\Delta\sigma = 13$ MPa for $M_w = 4.5$.

Note that in this study we obtain the stress drop parameter from one-corner source model as described by Brune (1971). However, different source models that characterize the radiated spectra are essential in the predictive relationships for large events at low frequencies. Some studies revealed the tendency of the Brune spectral model (1970, 1971) over-predicting low-frequency spectral amplitudes of large earthquakes (Atkinson & Silva 1997; Atkinson & Boore 1997). At the same time, many other studies demonstrated the Brune source spectrum is efficient in predicting the high-frequency ground motions through a stochastic approach (Hanks & McGuire 1981; Boore 1983; Silva & Darragh 1995). Boatwright & Choy (1992) and Atkinson & Boore (1997) realized that a two-corner-frequency spectral model alters the spectra of large intraplate events better than Brune model. In our study, we used a single corner-frequency model essentially to be consistent with the Stochastic-Method SIMulation SMSIM software (Boore 1996, 2003), this latter using the Brune (1971) values that have been adopted in the ground-motion predictions (see following section).

As it is seen in Fig. 5(b) we exposed a clear trade-off between the Brune stress parameter, $\Delta\sigma$ and κ. We compared averaged excitations terms with a series of theoretical source spectra computed using two κ parameters (0.04 and 0.004 s) together with three Brune stress parameters (1, 10 and 30 MPa). The spectral amplitude decay is controlled by the high frequency attenuation so that the κ_{eff} parameter is totally responsible of the behaviour at high frequency observed on small earthquakes. Conversely, the effect of the stress drop is stronger for the largest earthquakes. Therefore, we first obtained κ by performing a best fit analysis using an average spectral shape obtained from small earthquakes of magnitude between M2.0 and 2.5. Then we used an appropriate stress drop parameter to adjust the spectral levels at larger magnitudes ($M_w \sim 3.5$).

Additionally, the computation of moment magnitudes of several events in the data set were used to properly calibrate the source scaling. We used moment tensor solutions computed by using the 'Cut and Paste' method which employs a grid search technique to determine the source depth, moment magnitude and focal mechanisms (D'Amico *et al.* 2010, 2011).

Site terms

Fig. 6 shows the site terms recorded at the reference hypocentral distance by the network at each site. This result may present the quality check of the entire data set and results, as well as the verification of the instrument calibration accuracy. The site term represents the deviation from the mean seismic spectrum at each station, which is caused by the shallow physical properties related to local geology at the recording site. Since the site terms promote to trade-off with the empirical excitation source terms, they cannot be used properly in the present form. We stress that any systematic behaviour alter the site terms would be evolved into the excitation source terms of Figs 5(a) and (b), caused by the constrains adopted for the inversion process. However, the variability observed between individual site terms can be performed to quantify the uncertainties on our ground motions estimations. Although there exists methods (Malagnini *et al.* 2004, 2007, 2014a) to lower or ignore the implicit trade-off between excitation and site terms those are not applied in the present case.

ESTIMATION OF THE HIGH-FREQUENCY GROUND-MOTION PARAMETERS

We predict ground shaking levels as a series of ground-motion parameters, PGA, PGV and SA, through the RVT using the empirical excitation/source model, regional and site specific attenuation functions, and the estimated ground-motion duration following the Boore's (1996) SMSIM stochastic ground-motion model. The predictions are computed using the suite of source parameters computed in this study together with those the extrapolated stress parameters summarized in Table1, coupled with a generic rock site amplification factors ($V_{s30} = 760$ m s^{-1}, Boore 2016) using empirically obtained high-frequency attenuation parameter, obtained as 0.04 s. The reason why the generic rock site factors was assumed in our study, is that the estimated κ value (0.04 s) is consistent

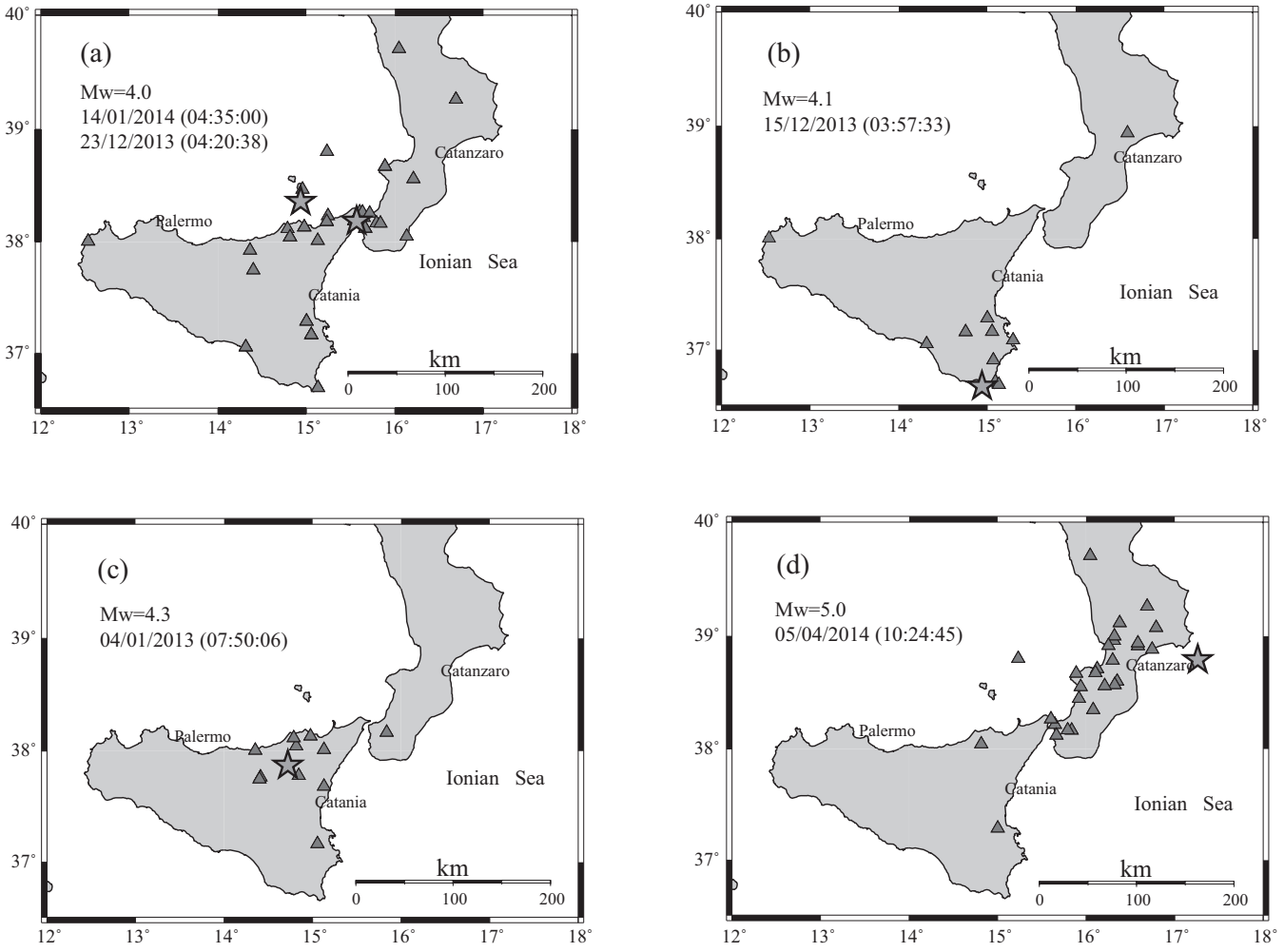

Figure 8. Earthquakes recorded by the Strong Motion Network (RAN) belonging to the Department of the Italian Civil Protection Agency in the study area, that are not used for the regression analysis but used for the validations; (a) 2014 January 14 (04:35:00), Latitude 38.362, Longitude 14.936, $h = 11$ km, $M_w = 4.0$; 2013 December 23 (04:20:38) $h = 7$, Lat 38.186, Lon 15.568, $M_{w=}$ 4.0; (b) 2013 December 15 (03:57:33), Latitude 36.671, Longitude 14.941, $h = 10.3$, $M_w = 4.1$; (c) 2013 January 4 (07:50:06), Latitude 37.873, Longitude 14.722, $h = 10.1$ km, $M_w = 4.3$; (d) 2014 April 5 (10:24:45), Latitude 38.793, Longitude 17.26, $h = 65.7$, $M_w = 5.0$. The epicentral locations of the earthquakes used for the validation analysis are given by stars. The locations of the strong-motion stations are given by triangles.

Table 1. High-frequency ground-motion model parameters.

$C = R_{\Theta\Phi} VF/4\pi\rho\beta^3$
$R_{\Theta\Phi} = 0.55$; $V = 0.707$; $F = 2.0$; $\rho = 2.8$ g cm^{-3}; $\beta = 3.5$ km s^{-1}
$s(f) = 1/[1 + (f/f_c)^2]$
$f_c = 0.49 \times 10^6\ \beta\ (\sigma/M_o)^{1/3}$ Hz
$_\omega = 2.0, 3.0, 4.0, 4.5$, $\Delta\sigma = 1, 5, 7, 13$ (empirical determined)
$_\omega = 5.0, 6.0, 7.0$; $\Delta\sigma = 20$ MPa (extrapolated)
$\kappa_{\text{eff}} = 0.04$ s
$Q(f) = 160(f)^{0.35}$
$g(r) = r^{-1.0}$ $r \le r_o$ 50 km
$g(r) = (1/r_o)(r_o/r)^{0.8}$ $r > r_o$
$F_{\max} = 100$ Hz
Generic Rock site amplification ($V_{s30} = 760$ m s^{-1}).

with the average value of $\kappa = 0.035$–0.04 s determined by Boore (2003) and Boore & Joyner (1997) in the western United States using the specific shear-wave velocity profile based on averaged shear wave velocities at 30 m depth, $V_{s30=}$ 760 m s^{-1} though the quarter-wavelength approach. Several models are developed that combine V_{s30} and κ scaling from hard-rock to soft-rock demonstrating the correlation beneath a given site between the shear wave velocity profile and the high frequency attenuation parameter (Campell *et al.* 2014, Ktenidou & Abrahamson 2016).

In fact, the aim of this study is demonstrating that weak-motion-based attenuation models, together with the source and site scaling may be used to estimate the ground-motion parameters as function of distance, magnitude and frequency more precisely (Malagnini *et al.* 2011; D'Amico *et al.* 2012).

As the four earthquakes registered by the Italian Strong-Motion Network (RAN) given in Fig. 8 were not included in the database driven for the prediction, we have used these events as a validation test. We thus extrapolate predictions for earthquakes only for more than a half magnitude unit above the largest earthquake in the calibration data set. Fig. 8 shows the location of recording site for events available only in the moment magnitude range 4.0-4.2 and 5.0.

Therefore, we attempt to extrapolate our results into larger magnitudes up to M 7.0, beyond the magnitude range that consists the database used in our regressions, for applicability to the seismic hazard assessment in the region. Since we do not have either the

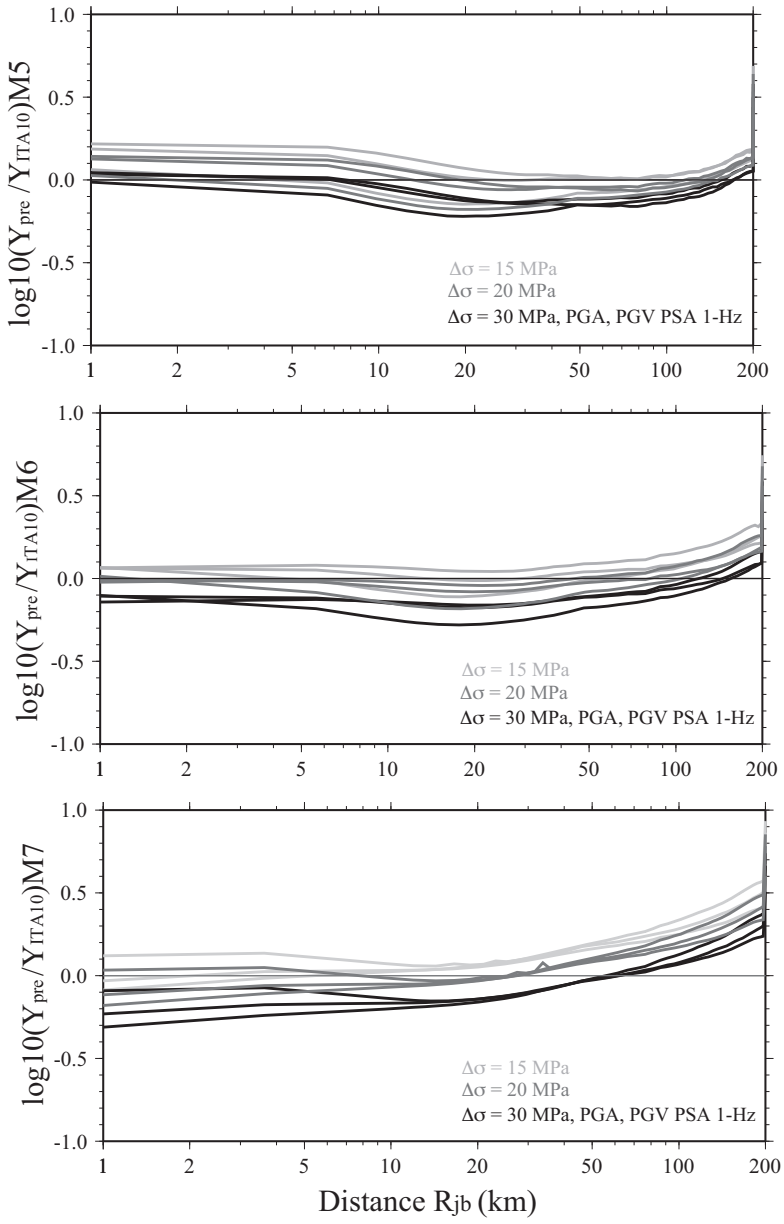

Figure 9. Residuals for the three magnitudes of events; (a) *M* 5.0, (b) *M* 6.0 and (c) *M* 7.0 between the predicted ground-motion parameters for three stress drop parameters ($\Delta\sigma$ 15, 20 and 30 MPa) and the selected GMPE, ITA10 derived by Bindi *et al.* (2011), plotted as functions of R_{jb} distance, in natural log units.

strong- or the weak-motion recordings for larger magnitudes we compare our ground-motion levels with those some from recently derived GMPEs. We adopt an attenuation equation from the Italian database derived by Bindi et *al.* (2010 and 2011), as a reference model for the B site class (V_{s30} = 360–800 m s^{-1}), classified according to Eurocode8, EC8 (CEN 2003). Regarding to the stress drop scaling with larger magnitudes (in our case M_w>4.5), we select two different stress models: (1) variable stress parameter with values of 10, 15, 20, 25, 30, 35 and 40 MPa for $M > 4.5$ events; (2) the constant stress parameter, 13 MPa which is equal to that of *M* 4.5 the stress drop value obtained in this study from the excitation terms (Fig. 5a curves with grey colours).

In order to assess the level of fit between predictions and the reference model ITA10, we calculate residuals, *R* at each R_{JB} distance *j,* as

$$R_j(\Delta\sigma) = \ln\left(Y_j, \text{GMPE}\right) - \ln\left(\bar{Y}(\Delta\sigma i)\, j, \text{SIM}\right), \quad (12)$$

where *Y* is the considered parameter (PGA, PGV or SA) from the ITA model. indicates, for the distance *j,* the predicted ground-motion parameters calculated using the stochastic approach. The model bias $B(\Delta\sigma_i)$ for a list of stress drop parameters was also computed by summing the residuals over all distances:

$$\text{B}(\Delta\sigma_i) = 1/N \sum_{j=1}^{N} (R_j(\Delta\sigma_i)). \quad (13)$$

A perfect match between the ITA10 and predicted model would have R_j= 0, whereas a negative residual shows an over prediction of the simulations with respect to the ITA10 model from GMPEs. In Figs 9(a)–(c), we present the residuals as a misfit between the reference ITA10 model and the predictions that are estimated using

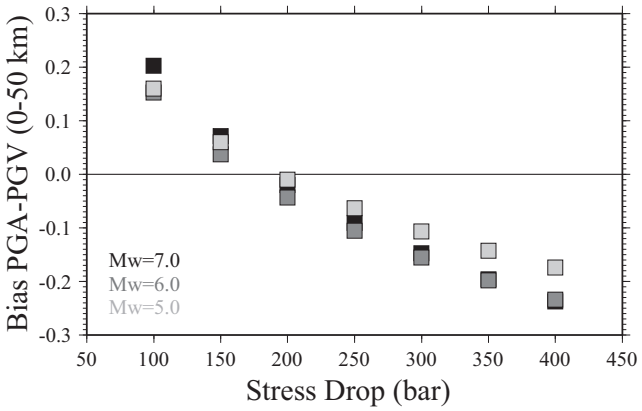

Figure 10. Comparison of model bias from the stochastic based ground-motion predictions calculated using a series of stress drop parameters with the selected GMPEs derived by Bindi *et al.* (2011) that was taken as a reference model over three magnitudes *M* 5.0, 6.0 and 7.0.

three different stress drop parameters (15, 20 and 30 MPa), as a function of distance for the selected ground-motion parameters (PGA, PGV and SA-1 Hz) for three magnitudes, *M* 5.0, 6.0 and 7.0, respectively. Stress drop parameter is sensitive at the larger magnitudes where the misfit decreases compare to that of *M* 5.0 at both closest ($R < 5$ km) and longer distances ($R < 100$ km).

However, Fig. 10 demonstrates the residuals computed using eq. (13) by averaging the residuals for the near and intermediate distances ($R_{JB} < 50$ km) considering the PGA and PGV values for the various stress drop parameters at three magnitudes and the best one that of close to zero, $\Delta\sigma = 20$ MPa which provides a better fit to the reference ITA10 model.

Figs 11(a)–(c) show the comparisons between the observed ground-motion parameters from those earthquakes recorded in the area, reference ITA10 model and the predictive model derived using the stress drop values $\Delta\sigma = 2.0$ MPa for events $M < 4.5$ and $\Delta\sigma = 20$ MPa for events $M > 4.5$. We stress that the smaller size magnitude $M < 4.5$ earthquakes cannot be explained by large stress drop of 20 MPa and above since they perfectly agree with the observed data.

We demonstrate that a stochastic model based on region-specific attenuation and source parameters provides a good fit to the registered data with magnitudes 4.0, 4.2 and 4.3 events, at distances of up to approximately 250 km (Figs 11a–d) while ITA10 model tends to over predict the shaking at those magnitudes. This is a good validation and of the predictive capability of the presented model at least for the small events. On the contrary the estimates of PGA for magnitude 5.0 event is underestimated by the ITA10 and the predicted model (Fig. 11a) while both models are in good agreement with observed PGV and SAs (Figs 11b–d). In generally, the predicted ground motions (PGAs, PGVs and SA) decay faster than the ITA10 model, at both moderate and large distances. The faster attenuation of ground motion is in agreement with the observed data at least for magnitudes between *M* 4.0 and 5.0 events. In this case the difference of PGA and the agreement at lower frequencies can be easily attributed to the fact that the earthquake hypocentral depth is 65 km, but our data set used to retrieve the crustal attenuation model does not contain any event deeper than 30 km. It is fair to point out that there are not several events in the area with magnitude greater than 5.0 so no other comparisons were possible.

In order to validate our ground-motion prediction for large earthquake ($M_w \geq 5.0$) we further simulated PGA values for 16 historical earthquakes occurred in the study area (Fig. 12; Table 2). More than eight hundred values have been simulated and compared with observed data available on the Italian Macroseismic Database (https://emidius.mi.ingv.it/CPTI15-DBMI15) by using the relationship between the IMCS and PGA, proposed by Locati *et al.* (2016) for Italian territory. As shown in Fig.12 our simulated values are in good agreement with the intensity reported by the estimates in the Italian Macro-seismic Database. However, the differences between the observed and simulated intensity values can be ascribed to the fact that PGA is surely affected by local site conditions and macroseismic data usually do not take into account possible structural problems of building stock.

CONCLUDING REMARKS

We have characterized the ground velocity distance scaling in the frequency range 0.25–20 Hz and in the distance range from 10 to 250 km in the Sicily Channel and around Maltese Islands. The attenuation characteristics are determined only on regional seismic events recorded by the stations of the regional network. They thus represent the average effects for shear and surface wave attenuation in the region. The inverted empirical excitation at the 20 km reference distance was inferred from spectral values for earthquake magnitudes between *M* 2.0 and *M* 4. The excitation spectra of seismic events obtained from the regressions previously described were suitably fit by using the model for wave propagation model shown through eqs (6) and (7). We completely removed the empirical excitation terms from the propagation model by using the constraint in eq. (2). For the spectral fit we included: (i) a single-corner frequency Brune spectral model adding a stress parameter increasing at increasing earthquake's magnitude up to larger magnitudes (*M* 7.0) more beyond the magnitudes of the empirical database (M_{wmax} 4.5); (ii) a roll-off parameter $\kappa = 0.04$ s for high frequencies together with the site amplifications as given by Boore (2016) for a generic rock site, $V_{s30} = 760$ m s^{-1}. While intermediate-to-high frequencies are sensitive to changes in the stress drop parameter, low frequencies may be sensitive to the chosen spectral model (e.g. single- versus double-corner frequency). However, since our database is mainly composed of small magnitude events (maximum magnitude being 4.5), the Brune spectral model is simply utilized to calibrate the stress drop parameter matching that with the excitation source term. We observed that the stress parameter increases with increasing magnitudes from *M* 2.0 to *M* 4.5, with the stress drop values of 2.0 and 13 MPa, respectively. However, we would like to stress that the extrapolated stress drop parameter for larger events (*M* 5.0 up to *M* 7.0) obtained in this study may imply large uncertainties at the larger magnitudes (see Figs 5b and 10d) considering the lack of large magnitude events in the database. The stress drop obtained for events with $M > 4.5$–5.0 is constant, being 20 MPa up to larger *M* 7.0 magnitude events while it increases with increasing magnitude up to *M* 5.0 and then becomes constant. This value is validated comparing the predicted PGAs against the observed data available on the Italian Macroseismic Database for larger events, showing good agreement with the reported intensity. Nevertheless, it is essential having a complete weak-motion data set that covers large range of magnitude events (let say *M* 2.0–7.0) for an accurate ground-motion prediction particularly in regions where strong-motion data are not available. In this study we demonstrate that the weak-motion-based region-specific high-frequency spectral parameters can be used to

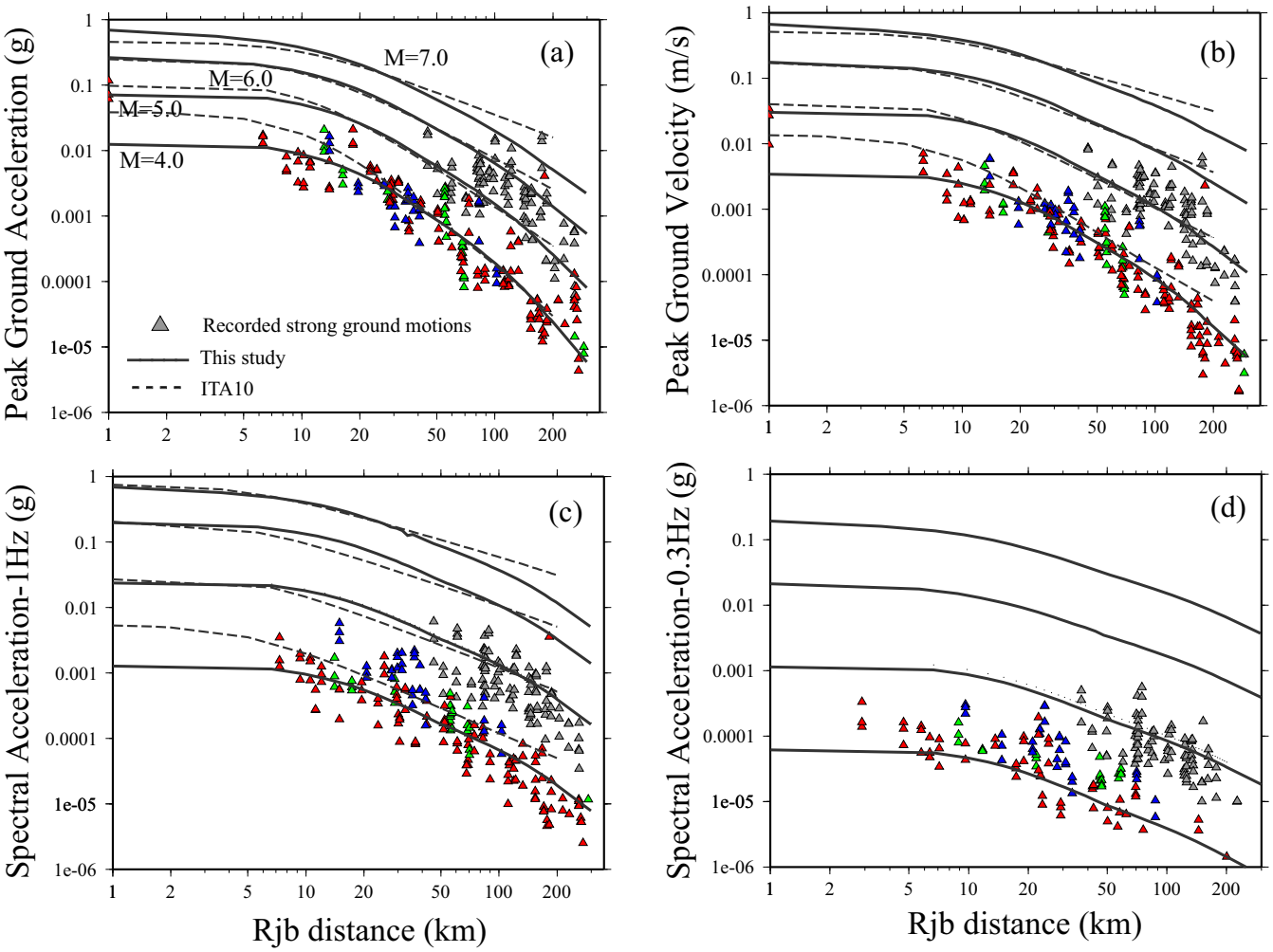

Figure 11. Comparisons of observed, predicted and reference model ground-motion parameters in terms of (a) PGA (g); (b) PGV (cm s^{-1}); (c) SA (0.3 Hz) and (d) SA (1 Hz). The reference model (dashed lines) is adopted from Bindi *et al.* (2011) considering the B site class that is related to $V_{s30} = 360$–800 m s^{-1}, following the Eurocode8, EC8, (CEN 2003). The simulated values (continuous lines) are obtained through the RVT utilizing the SMSIM computer code (Boore 1996). The simulated PGA and PGV values were estimated for earthquakes reported in Fig.7 (grey triangles represent the observed data for $M_w = 5.0$ while the red, green and blue triangles represent the observed ground-motion parameter for the events with magnitude 4.0, 4.1 and 4.3) using the parameters derived in this study (see spectral parameters in Table 1).

well predict the average ground-motion amplitudes through stochastic approach, presenting good agreement with the recorded events so for intermediate magnitudes (around M 4.1–4.5).

Furthermore, recently published papers (Akinci *et al.* 2014; Drouet & Cotton 2015; Edwards *et al.* (2016) have pointed out that the crustal and near-site attenuation as well as the source scaling are both region-dependent, thus it is crucial to perform regional studies for ground-motion prediction. Unfavourably there exit few or no information, as well as published scientific documents on the mentioned parameters for the study region. Di Bona *et al.* (1995) studied source and attenuation parameters for the 1990 Eastern Sicily earthquake (M 5.3), and found $\kappa = 0.040 \pm 0.005$ s using the data mostly recorded by the strong-motion stations located on the Iblean platform. In their study they fitted the *S*-wave acceleration spectra with a Brune source model for each recording (Boore 1996), calculating stress-drop parameters between 21 and 200 MPa. This variety of values for the stress drop and κ parameters was referred by the authors to crustal heterogeneities and near receiver amplification due to surface geology and topography. Our estimate of κ value is quite similar to computation by Di Bona *et al.* (1995).

Scognamiglio *et al.* (2005) have found different $Q(f)$ relations for a small region in Sicily, with higher Q and κ values respect to values found in this study. This discrepancy could be linked with: (i) the limited number of data and particularly short range of frequency used by Scognamiglio *et al.* (2005) in a relatively smaller area compared to one studied in this study; (ii) the different geologic and tectonic settings between the two areas.

Our results contribute to the perception that the variation of the stress drop value as well as parameters describing the crustal attenuation is of primary importance in the strong ground-motion predictions, in both deterministic and stochastic methods. These methods are very useful when not enough real recordings are available to assess ground motion at large magnitude (Edwards & Fäh 2013; Rietbrock *et al.* 2013). In this study we provide the weak-motion-based region-specific high-frequency spectral parameters may be utilized estimating the ground-motion amplitudes and parameters through stochastic and deterministic methods for future earthquakes in the Sicily Channel. Finally, we conclude that the uncertainties related to region-specific ground-motion prediction equations may be reduced by using extensive and more complete weak-motion data

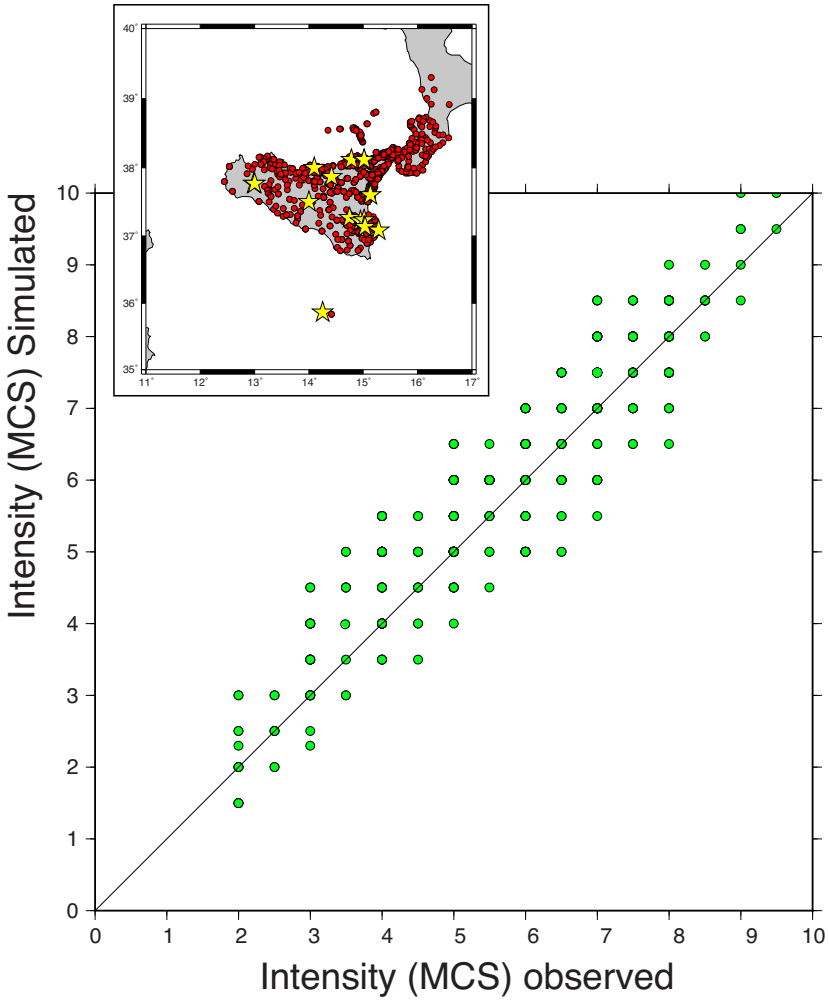

Figure 12. Comparison of observed MCS intensity values versus simulated. The latter were converted using Locati *et al.* (2016) relationship. Note that the number of points represented by this graph is actually larger than the number of points shown, since any point may represent multiple occurrences of a given observed/simulated intensity pair. The inset shows the epicentral location of historical earthquakes reported in Table2.

Table 2. Source parameters of the historical earthquakes used in this study.

Date	Time	Lat	Lon	Io	No. of Sites	Equivalent magnitude
1 9 1726	21:55	38.117	13.35	7.5	8	5.6
5 3 1823	16:37	38	14.1	8	107	5.7
31 10 1967	21:08:07	37.867	14.417	8	60	5.6
25 8 1613	5:00	38.117	14.783	8	2	5.6
10 3 1786	14:10	38.1	15.017	9	10	6.2
15 4 1978	23:33:47	38.117	15.017	8	333	5.7
20 2 1818	18:15	37.6	15.133	9.5	128	6.2
3 10 1624	17:00	37.267	14.75	8	4	5.6
4 2 1169	7:00	37.217	14.95	10	10	6.4
10 12 1542	15:15	37.233	15.017	10	32	6.8
11 1 1693	13:30	37.133	15.017	11	185	7.4
9 1 1693	21:00	37.133	15.033	8.5	30	6.2
7 6 1125	11:00	37.083	15.283	8.5	1	5.8
1 9 1295	3:00	37.5	14	8.5	1	5.8
15 1 1968	2:01:09	37.767	12.983	10	163	6.5
15 1 1968	1:33:02	37.767	13	8	15	5.6

set composed of waveforms recorded both at local and regional distances produced by large earthquake sequences that cover both large distance and magnitude ranges.

ACKNOWLEDGEMENTS

This study was partially supported by SIMIT Project co-financed by the European Union European Regional Development under the Italia-Malta Cross-Border Cooperation Programme, 2007–2013. We would like to thank Istituto Nazionale di Geofisica e Vulcanologia (INGV) and Department of Civil Protection (DPC) for the efforts towards deploying seismic stations and for providing all kinds of seismological data and earthquake information for our scientific research and study. We appreciate David Boore for providing the SMSIM computer code. We thank Luca Malagnini of INGV, Italy and Robert B. Herrmann of Saint Louis University, USA and Pauline Galea of University of Malta for their helpful discussions. The Generic Mapping Tools version 4.2.1 (www.soest.hawwai.edu/gmt) and the Seismic Analysis Code (SAC) software are elaborated to prepare many plots, figures and seismic macros, respectively, in this work. Comments by the Jain Virieux, Salvatore De Lorenzo and an anonymous reviewer improved the final version of the manuscript.

REFERENCES

Abrahamson, N., Silva, W. & Kamai, R., 2014. Summary of the ASK14 ground motion relation for active crustal regions, *Earthq. Spectra,* **30,** 1025–1055.

Aki, K., 1980. Attenuation of Shear-waves in the Lithosphere for Frequencies from 0.05 to 25 Hz, *Phys. Earth Planet. Inter,* **21,** 50–60.

Aki, K., 1981. Attenuation and scattering of short-period seismic waves in the lithosphere, in *Identification of Seismic Sources—Earthquake or Underground Explosion,* eds Usebye, E.S. & Mykkeltveit, S., ATO Advanced Study Institutes Series (Series C — Mathematical and Physical Sciences), Vol. **74,** Springer.

Aki, K. & Richards, P.G., 2002. *Quantitative Seismology,* 2nd edn, pp. 678, University Science Books.

Akinci, A., Malagnini, L. & Herrmann, R.B., 2014. High-frequency attenuation in the lake van region, Eastern Turkey, *Bull. seism. Soc. Am.,* **104**(3), 1400 –1409.

Akinci, A., Malagnini, L., Herrmann, R.B., Gok, R. & Sorensen, M., 2006. Ground motion scaling in the Marmara Region, Turkey, *Geophys. J. Int.,* **166,** 635–651.

Akkar, S., Sandikkaya, M.A. & Bommer, J.J., 2014a. Empirical ground motion models for point- and extended-source crustal earthquake scenarios in Europe and the Middle East, *Bull. Earthq. Eng.,* **12,** 359–387.

Akkar, S., Sandikkaya, M.A. & Bommer, J.J., 2014b. Erratum to "Empirical ground-motion models for point- and extended-source crustal Comprehensive Comparison among CB14 and Pan-European GMPEs 2101 earthquakes in Europe and the Middle East", *Bull. Earthq. Eng.,* **12,** 389–390.

Anderson, J.G & Hough, S.E., 1984. A model for the shape of the Fourier amplitude spectrum of acceleration at high frequencies, *Bull. seism. Soc. Am.,* **74**(5), 1969–1993.

Andrews, D.J., 1986. Objective determination of source parameters and similarity of earthquakes of different size, in *Earthquake Source Mechanics,* pp. 259–267, eds Das, S., Boatwright, J. & Scholz, C.H., American Geophysical Union.

Argnani, A. & Bonazzi, C., 2005. Malta Escarpment fault zone offshore eastern Sicily: Pliocene-Quaternary tectonic evolution based on new multichannel seismic data, *Tectonics,* **24,** (4), TC4009, doi:10.1029/2004TC001656.

Atkinson, G.M. & Boore, D.M., 1995. Ground-motion relations for eastern North America, *Bull. seism. Soc. Am.,* **85,** 17–30.

Atkinson, G.M. & Boore, D.M., 1997. Stochastic point-source modeling of ground motions in the Cascadia region, *Seismol. Res. Lett.,* **68,** 74–85.

Atkinson, G.M. & Boore, D.M., 2006. Earthquake ground-motion prediction equations for Eastern North America, *Bull. seism. Soc. Am.,* **96,** 2181–2205.

Atkinson, G.M. & Silva, W., 1997. An empirical study of earthquake source spectra for California earthquakes, *Bull. seism. Soc. Am.,* **87,** 97–113.

Baccheschi, P. & D'Amico, S., 2014. Subduction, volcanism, collision, orogenesis and faults: How do they shape the central Mediterranean region?, *J. Geodyn.,* **82,** 1–4.

Bartels, R. & Conn, A., 1980. Linearly constrained discrete l1 problems, *ACM Trans. Math. Softw.,* **6,** 594–608.

Bianca, M., Monaco, C., Tortorici, L. & Cernobori, L., 1999. Quaternary normal faulting in southeastern Sicily (Italy): a seismic source for the 1693 large earthquake, *Geophys. J. Int.,* **139,** 370–394.

Bindi, D., Luzi, L., Massa, M. & Pacor, F., 2010. Horizontal and vertical ground motion prediction equations derived from the Italian Accelerometric Archive (ITACA), *Bull. Earthq. Eng.,* **8**(5), 1209–1230.

Bindi, D., Massa, M., Luzi, L., Ameri, G., Pacor, F., Puglia, R. & Augliera, P., 2014a. Pan-European ground-motion prediction equations for the average horizontal component of PGA, PGV, and 5%-damped PSA at spectral periods up to 3.0 s using the RESORCE dataset, *Bull. Earthq. Eng.,* **12,** 391–430.

Bindi, D., Massa, M., Luzi, L., Ameri, G., Pacor, F., Puglia, R. & Augliera, P., 2014b. Erratum to "Pan-European ground-motion prediction equations for the average horizontal component of PGA, PGV, and 5%-damped PSA at spectral periods up to 3.0 s using the RESORCE dataset", *Bull. Earthq. Eng.,* **12,** 431–448.

Bindi, D., Pacor, F., Luzi, L., Puglia, R., Massa, M., Ameri, G. & Paolucci, R., 2011. Ground motion prediction equations derived from the Italian strong motion database, *Bull. Earthq. Eng.,* **9,** 1899–1920.

Boatwright, J. & Choy, G., 1992. Acceleration source spectra anticipated for large earthquakes in Northeastern North America, *Bull. seism. Soc. Am.,* **82,** 660–682.

Boatwright, J., Fletcher, J.B. & Fumal, T.E., 1991. A general inversion scheme for source site, and propagation characteristics using multiply recorded sets of moderate-sized earthquakes, *Bull. seism. Soc. Am.,* **81,** 1754–1782.

Bommer, J.J. & Martinez-Pereira, A., 1999. The effective duration of earthquake strong motion, *J. Earthq. Engi.,* **3**(2), 127–172.

Bonson, C.G., Childs, C., Walsh, J.J., Schopfer, M.P. & Carboni, V., 2007. Geometric and kinematic controls on the internal structure of a large normal fault in massive limestones: The Maghlaq Fault, Malta, *J. Struct. Geol.,* **29**(2), 336–354.

Boore, D.B., 2003. Prediction of ground motion using the stochastic method, Pure and Applied, *Geophysics,* **160,** 635–676, Available from the online publications link on https://profile.usgs.gov/professional/mypage.php?name=boore.

Boore, D.M., 1983. Stochastic simulation of high-frequency ground motions based on seismological models of the radiated spectra, *Bull. seism. Soc. Am.,* **73,** 1865–1894.

Boore, D.M., 1996. SMSIM – Fortran Programs for Simulating Ground Motions from Earthquakes: Version 1.0, U.S. Geol. Surv. Open-File Rept. 96-80-A, 96-80-B, 73 pp.

Boore, D.M., 2005. SMSIM—Fortran programs for simulating ground motions from earthquakes: version 2.3—a revision of OFR 96– 80–A, available at: http://www.daveboore.com/smsim.

Boore, D.M., 2014. What do data used to develop ground-motion prediction equations tell us about motions near faults? *Pure appl. Geophys.,* **171,** 3023–3043.

Boore, D.M., 2016. Determining generic velocity and density models for crustal amplification calculations, with an update of the Boore and Joyner (1997) generic site amplification for Vs(30) = 760 m/s, *Bull. seism. Soc. Am.,* **106,** 316–320.

Boore, D.M. & Joyner, W.B., 1984. A note on the use of random vibration theory to predict peak amplitudes of transient signals, *Bull. seism. Soc. Am.,* **74**(5), 2035–2039.

Boore, D.M. & Joyner, W.B., 1997. Site amplifications for Generic Rock Sites, *Bull. Seismol. Soc. Am.,* **87,**327 341.

Bora, S.S., Scherbaum, F., Kuehn, N., Stafford, P. & Edwards, B., 2015. Development of a response spectral ground-motion prediction equation (GMPE) for seismic-hazard analysis from empirical Fourier spectral and duration models, *Bull. seism. Soc. Am.,* **105,** 2192–2218.

Boschi, E., Ferrari, G., Gasperini, P., Guidoboni, E., Smiriglio, G. & Valensise, G. eds, 1995, *Catalogo dei forti terremoti in Italia dal 461 a.C. al*

1980, ING–SGA, pp. 973.
Bozorgnia, Y. *et al.*, 2014. NGA-West2 research project, *Earthq. Spectra,* **30,** 973–987.
Brune, J., 1970. Tectonic stress and the spectra of seismic shear waves from earthquakes, *J. geophys. Res.,* **75,** 4997–5009.
Brune, J., 1971. Correction, *J. geophys. Res.,* **76,** 5002.
Campbell, K.W. & Bozorgnia, Y., 2014. NGA-West2 ground motion model for the average horizontal components of PGA, PGV, and 5% damped linear acceleration response spectra, *Earthq. Spectra,* **30,** 1087–1115.
Carver, D. & Hartzel, S.H., 1995. Earthquake site response in Santa Cruz, California, *Bull. seism. Soc. Am.,* **86,** 55–65.
Castro, R., Anderson, J. & Singh, S., 1990. Site response, attenuation and source spectra of Swaves along the Guerrero, Mexico, subduction zone, *Bull. seism. Soc. Am.,* **80**(6), 1481–1503.
Cello, G., Crisci, G.M., Marabini, S. & Tortorici, L., 1985. Transtensive tectonics in the Strait of Sicily: structural and volcanological evidence from the island of Pantelleria, *Tectonics,* **4,** 311–322.
CEN, 2003. prEN 1998-1-Eurocode 8: design of structures for earthquake resistance—part 1: general rules, seismic actions and rules for buildings. Draft No 6, Doc CEN/TC250/SC8/N335, January 2003, Brussels.
Chiou, B.S.-J. & Youngs, R.R., 2014. Update of the chiou and youngs NGA model for the average horizontal component of peak ground motion and response spectra, *Earthq. Spectra,* **30,** 1117–1153.
D'Amico, S., Akinci, A. & Malagnini, L., 2012. Predictions of high-frequency ground-motion in Taiwan based on weak motion data, *Geophys. J. Int.,* **189,** 611–628.
D'Amico, S., Lombardo, G. & Panzera, F., 2013. Seismicity of the Mediterranean region and mitigation of earthquake losses, *Phys. Chem. Earth,* **63,** 1–2.
D'Amico, S., Orecchio, B., Presti, D., Gervasi, A., Guerra, I., Neri, G., Zhu, L. & Herrmann, R.B., 2011. Testing the stability of moment tensor solutions for small and moderate earthquakes in the Calabrian-Peloritan arc region, *Boll. Geofis. Teor. Appl.,* **52,** 283–298.
D'Amico, S., Orecchio, B., Presti, D., Zhu, L., Herrmann, R.B. & Neri, G., 2010. Broadband waveform inversion of moderate earthquakes in the Messina straits, Southern Italy, *Phys. Earth planet. Inter.,* **179,** 97–106.
Dart, C.J., Bosence, D.W.J. & McClay, K.R., 1993. Stratigraphy and structure of the Maltese Islands, *J. Geol. Soc.,* **150,** 1153–1166.
Di Bona, M., Cocco, M., Rovelli, A., Berardi, R. & Boschi, E., 1995. Analysis of strong-motion data of the 1990 Eastern Sicily earthquake, *Ann. Geofis.,* **38**(2), 283–300.
Douglas, J., 2011. Investigating possible regional dependence in strong ground motions, in *Earthquake Data in Engineering Seismology. Geotechnical, Geological, and Earthquake Engineering,* Vol., **14,** eds Akkar, S., Gülkan, P. & van Eck, T., Springer.
Drouet, S. & Cotton, F., 2015. Regional stochastic GMPEs in low-seismicity areas: scaling and aleatory variability analysis—application to the french alps, *Bull. seism. Soc. Am.,* **105**(4), 1883–1902.
Edwards, B., Cauzzi, C., Danciu, L. & Fäh, D., 2016. Region-specific assessment, adjustment, and weighting of ground-motion prediction models: application to the 2015 swiss seismic-hazard maps, *Bull. seism. Soc. Am.,* **106,** (4)1840–1857.
Edwards, B. & Fäh, D., 2013. A stochastic ground-motion model for Switzerland, *Bull. seism. Soc. Am.,* **103**(1), 78–98.
Edwards, B., Rietbrock, A., Bommer, J.J. & Baptie, B., 2008. The acquisition of source, path, and site effects from microearthquake recordings using Q tomography: application to the United Kingdom, *Bull. seism. Soc. Am.,* **98,** (4) 1915–1935.
Finetti, I., 1982. Structure, stratigraphy and evolution of the central Mediterranean, *Boll. Geofis. Teor. Appl.,* **24,** 247–312.
Galea, P., 2007. Seismic history of the Maltese islands and considerations on seismic risk, *Ann. Geofis.,* **50,** 725–740.
Gardiner, W., Grasso, M. & Sedgeley, D., 1995. Plio-Pleistocene fault movement as evidence for mega-block kineatics within the Hyblean-Malta plateau, Central Mediterranean, *J. Geodyn.,* **19**(1), 35–51.
Hanks, T.C. & Kanamori, H., 1979. A moment magnitude scale, *J. geophys. Res.,* **84**(B5), 2348–2350.
Hanks, T.C. & McGuire, R.K., 1981. The character of high frequency strong ground motion, *Bull seism. Soc. Am,*. **71,** 2071–2095.
Hartzell, S.H., 1992. Site response estimation from earthquake data, *Bull. seism. Soc. Am.,* **82,** 2308–2327.
Idriss, I.M., 2014. An NGA-West2 empirical model for estimating the horizontal spectral values generated by shallow crustal earthquakes, *Earthq. Spectra,* **30,** 1155–1177.
Iwata, T. & Irikura, K., 1988. Source parameters of the 1983 Japan sea earthquake sequence, *J. Phys. Earth,* **36**(4), 155–184.
Knopoff, L. & Hudson, J.A., 1967. Frequency dependence of amplitudes of scattered elastic waves, *J. acoust. Soc. Am.,* **42,** 18–20.
Ktenidou, O.J. & Abrahamsson, N.A., 2016. Empirical Estimation of High-Frequency Ground Motion on Hard Rock, *Seismological Research Letters,* **87,** (6), 1465–1478.
Locati, M., Gomez Capera, A.A., Puglia, R. & Santulin, M., 2016. Rosetta, a tool for linking accelerometric recordings and macroseismic observations: description and applications, *Bull Earthquake Eng,* doi:10.1007/s10518-016-9955-y.
Lorenzo, S., Bianco, F. & Del Pezzo, E., 2013. Frequency dependent Qα and Qβ in the Umbria-Marche (Italy) region using a quadratic approximation of the coda-normalization method, *Geophys. J. Int.,* **193,** 1726–1731.
Mahin, S.A., 1980, Effects of duration and aftershocks on inelastic design earthquakes, in *Proceedings of the Seventh World Conference on Earthquake Engineering,* Istanbul, *Vol. 5,* pp. 677–680.
Malagnini, L., Akinci, A., Mayeda, K., Herrmann, R.B. & Mercuri, A. 2011, Characterization of earthquake-induced ground motion from the L'Aquila seismic sequence of 2009, Italy, *Geophys. J. Int.,* **184,** 325–337.
Malagnini, L. & Hermann, R.B., 2000. Ground-motion scaling in the region of the Umbria- Marche earthquake of 1997, *Bull. seism. Soc. Am*., **90,** 1041–1051.
Malagnini, L., Hermann, R.B. & Koch, K., 2000. Regional ground motion scaling in central Europe, *Bull seism. Soc. Am,*. **90,** 1052–1061.
Malagnini, L., Herrmann, R.B., Munafò, I., Buttinelli, M., Anselmi, M., Akinci, A. & Boschi, E., 2012. The 2012 Ferrara seismic sequence: regional crustal structure, earthquake sources, and seismic hazard, *Geophys. Res. Lett.,* **39,** L19302, doi:10.1029/2012GL053214.
Malagnini, L., Mayeda, K., Akinci, A. & Bragato, P.L., 2004. Estimating absolute site effects, *Bull. seism. Soc. Am.,* **94,** 1343–1352.
Malagnini, L., Mayeda, K., Nielsen, S., Yoo, S.-H., Munafo', I., Rawles, C. & Boschi, E., 2014a. Scaling transition in earthquake sources: a possible link between seismic and laboratory measurements, *Pure appl. Geophys.,* **171,** 2685–2707.
Malagnini, L., Mayeda, K., Uhrhammer, R., Akinci, A. & Herrmann, R.B., 2007. A regional ground motion excitation/attenuation model for the San Francisco region, *Bull. seism. Soc. Am.,* **97,** 843–862.
Malagnini, L., Munafo', I., Cocco, M., Nielsen, S., Mayeda, K. & Boschi, E., 2014b. Gradual fault weakening with seismic slip: inferences from the seismic sequences of L'Aquila, 2009 and Northridge, 1994, *Pure appl. Geophys.,* **171,** 2709–2730.
Mitchell, B.J., 1981. Regional variation and frequency dependence of Qβ in the crust of the United States, *Bull. seism. Soc. Am.,* **71,** 1531–1538.
Newman, P., 1973. Divergence effects in a layered earth, *Geophysics,* **38**(3), 481–488.
NGA-East Project, 2015. - http://peer.berkeley.edu/ngaeast/.
Pedley, H.M., 1987. Controls on Cenozoic carbonate deposition in the Maltese Islands: review and interpretation, *Mem. Soc. Geol. Ital.,* **38,** 81–94.
Pezeshk, S., Zandieh, A. & Tavakoli, B., 2011. Hybrid empirical ground-motion prediction equations for eastern north America using NGA models and updated seismological parameters, *Bull. seism. Soc. Am.,* **101**(4), 1859–1870.
Phillips, W. & Aki, K., 1986. Site amplification of coda waves from local earthquakes in central California, *Bull. seism. Soc. Am.,* **76,** 627–648.
Pisconti, A., Del Pezzo, E., Bianco, F. & de Lorenzo, S., 2015. Seismic Q estimates in Umbria Marche (Central Italy): hints for the retrieval of a new attenuation law for seismic risk, *Geophys. J. Int.,* **201,** 1370–1382.
Raoof, M., Herrmann, R.B. & Malagnini, L., 1999. Attenuation and excitation of three component ground motion in southern California, *Bull. seism. Soc. Am.,* **89,** 888–902.
Reuther, C.D. & Eisbacher, G.H., 1985. Pantelleria Rift: crustal extension

in a convergent intraplate setting, *Geol. Rundsch.,* **74,** 585–597.
Rietbrock, A., Strasser, F. & Edwards, B., 2013. A stochastic earthquake ground motion prediction model for the United Kingdom, *Bull. seism. Soc. Am.,* **103**(1), 57–77, .
Rovida, R., Camassi, P., Gasperini, P. & Stucchi, M., 2011. *CPTI11, la versione 2011 del Catalogo Parametrico dei Terremoti Italiani,* INGV, http://emidius.mi.ingv.it/CPTI
Scognamiglio, L., Malagnini, L. & Akinci, A. 2005. Ground motion scaling in Eastern Sicily, *Bull. seism. Soc. Am.,* **95**(2), 568–578.
Silva, W. & Darragh, R.B., 1995, Engineering Characterization of Strong Ground Motion Recorded at Rock Sites, Final Report, United States, N. p., 1995. Print.
Tinti, S. & Armigliato, A., 2003. The use of scenarios to evaluate tsunami impact in South Italy, *Mar. Geol.,* **199**(3-4), 221–243.
Tinti, S., Armigliato, A. & Bortolucci, E., 2001. Contribution of tsunami data analysis to constrain the seismic source: the case of the 1693 Eastern Sicily earthquake, *J. Seismol.,* **5,** 41–61.
Tinti, S., Maramai, A. & Graziani, L., 2004. The new catalogue of Italian tsunamis, *Nat. Hazards,* **33**(3), 439–465.